nuclear fusion
IAEA

LETTER • OPEN ACCESS

Global saturation physics of ion temperature gradient turbulence in finite normalized pressure tokamaks

To cite this article: H. Masui *et al* 2022 *Nucl. Fusion* **62** 074001

View the article online for updates and enhancements.

You may also like

- Development of the PhysioVessel: a customizable platform for simulating physiological fluid resuscitation
David Berard, Saul J Vega, Sofia I Hernandez Torres et al.
- Effect of the relative shift between the electron density and temperature pedestal position on the pedestal stability in JET-ILW and comparison with JET-C
E. Stefanikova, L. Frassinetti, S. Saarelma et al.
- Gyrokinetic simulations of entropy transfer in high ion temperature LHD plasmas
T H Watanabe, H Sugama, M Nunami et al.

This content was downloaded from IP address 130.54.130.250 on 25/05/2022 at 07:26

OPEN ACCESS
IOP Publishing | International Atomic Energy Agency Nuclear Fusion
Nucl. Fusion **62** (2022) 074001 (6pp) https://doi.org/10.1088/1741-4326/ac667f

Letter

Global saturation physics of ion temperature gradient turbulence in finite normalized pressure tokamaks

H. Masui*, A. Ishizawa, K. Imadera, Y. Kishimoto and Y. Nakamura

Graduate School of Energy Science, Kyoto University, Uji 611-0011, Japan

E-mail: masui.hideaki.s14@kyoto-u.jp

Received 29 January 2022, revised 30 March 2022
Accepted for publication 12 April 2022
Published 26 April 2022

Abstract

Nonlinear saturation mechanism of ion-temperature-gradient turbulence at finite normalized pressure is identified by analysis of the nonlinear entropy transfer in global gyrokinetic simulations of the turbulence. Turbulence at such finite normalized pressure is electromagnetic and often exhibits non-saturation due to a lack of zonal flows by the influence of magnetic fluctuations of the turbulence in local gyrokinetic simulations. The present study identifies a new saturation mechanism caused by global entropy transfer due to turbulent $E \times B$ flow convection in real space. The convection of the entropy associated with the turbulence in the radial direction produces global zonal flows at the both sides of the most active region of the turbulence to avoid the effect of the magnetic fluctuations, and then global zonal-flow excitation is not suppressed, leading to a steady state of the turbulence.

Keywords: plasma turbulence, magnetic confinement fusion, nonlinear phenomena in plasmas, plasma fusion

(Some figures may appear in colour only in the online journal)

1. Introduction

Turbulence is known to be electromagnetic in finite normalized pressure (β) plasmas [1–6]. The understanding of electromagnetic turbulence is an important issue in magnetic confinement and in space and astrophysics [7, 8]; for instance, the β dependence of electromagnetic turbulent transport is critical for predicting the performance of fusion reactors, because it is related to the fusion reaction rate and also linked to the production of bootstrap current which is required to realize steady state operation of tokamaks. Whereas in low-β plasmas the zonal flow shear acts to regulate the ion-temperature-gradient (ITG) turbulence, it has often been observed that, at moderate-β, the ITG turbulence continues to grow without reaching a physically relevant level of saturation in many local gyrokinetic simulations of electromagnetic turbulence [2–4, 9–11]. For instance, the ITG turbulence continues to grow above $\beta = 1.2\%$, which is much lower than the critical β of the kinetic ballooning mode $\beta_{\rm crit}^{\rm KBM} = 2.5\%$, for the cyclone base case DIII-D parameters. The non-saturation is due to a lack of zonal flows and is known as the run-away/non-zonal-transition [9–11], and the suppression of zonal flows stems from stochastic magnetic field produced by the electromagnetic turbulence [12, 13]. On the other hand, recently, a saturation of KBM turbulence at high-β is observed in global

* Author to whom any correspondence should be addressed.

Original content from this work may be used under the terms of the Creative Commons Attribution 4.0 licence. Any further distribution of this work must maintain attribution to the author(s) and the title of the work, journal citation and DOI.

 © 2022 The Author(s). Published on behalf of IAEA by IOP Publishing Ltd

gyrokinetic simulations [14, 15]. The identification of a saturation mechanism for the ITG turbulence in finite-β regimes is important for understanding experimentally observed trends of β dependencies of confinement [16–20], and is the subject of the present work.

In this letter, we present that the saturation of the ITG turbulence at moderate-β is caused by global zonal-flow excitation due to the entropy transfer in real space by means of global gyrokinetic simulations. The mechanism of global zonal-flow excitation is examined by analysis of the nonlinear entropy/free-energy transfer from the ITG turbulence to the zonal flows in real space as well as wavenumber space. The radial convection of the entropy by turbulent $E \times B$ flow is found to play a key role in the saturation. The convection spreads the entropy of the turbulence from the peak of the fluctuation amplitude to the side of the peak in real space, and thus the entropy of the turbulence is transferred to the zonal flows not at the peak of the turbulence but at the side of the peak. As a result, the zonal-flow excitation is not suppressed by the influence of magnetic fluctuations of the turbulence. It is also found that the entropy is not only transferred to zonal flows but also to low toroidal wavenumber modes. These two nonlinear saturation mechanisms are the missing physics in the local simulations which exhibit the non-saturation of the turbulence at moderate-β.

2. Simulation model and entropy transfer analysis

We study the saturation mechanism of the ITG turbulence in finite-β tokamak plasma, using the global gyrokinetic simulation code GKNET [21, 22] which solves the gyrokinetic equation [23]

$$\frac{\partial h_s}{\partial t} = -[\chi_s, h_s] + L + C \tag{1}$$

for the non-adiabatic part of the distribution function h_s, the Poisson equation for the electrostatic potential ϕ, and Ampere's law for the parallel component of vector potential $A_\parallel$, where $\chi_s = \langle\phi\rangle_s - v_{Ts} v_\parallel \langle A_\parallel\rangle_s$, and the subscript s and $\langle\rangle_s$ denote particle species and a gyro-average, respectively. The normalization used in the equations is $(tv_{Ti}/R_0,\ \rho_{Ti}\nabla_\perp,\ v_\parallel/v_{Ts},\ F_{0s}v_{Ts}^3/n(r_0),\ \delta f_s R_0 v_{Ts}^3/(\rho_{Ti} n(r_0)),\ e\phi R_0/(\rho_{Ti} T_i(r_0)),\ A_\parallel R_0/(\rho_{Ti}^2 B_0),\ T_s/T_i(r_0)) \to (t, \nabla_\perp, v_\parallel, F_{0s}, \delta f_s, \phi, A_\parallel, T_s)$, where $\rho_{Ti} = v_{Ti}/\Omega_i$ and $v_{Ts} = \sqrt{T_{0s}/m_s}$. The nonlinear term is represented by the Poisson bracket $[f, g] = \mathbf{b} \cdot \nabla_\perp f \times \nabla_\perp g$, L denotes the linear driving terms of instabilities, and C is the collision term. We consider the cyclone base case like tokamak plasma [24], and the profiles are $q = 0.85 + 2.18(r/a)^2$, $n(r) = n_0 \exp\left[-\frac{\delta_r}{L_n}\tanh(\frac{r-r_0}{\delta_r})\right]$, and $T_s(r) = T_{0s} \exp\left[-\frac{\delta_r}{L_{Ts}}\tanh(\frac{r-r_0}{\delta_r})\right]$ with $r_0 = a/2$, $\delta_r = 0.3a$, $R_0/L_{Ts} = 6.66$, and $R_0/L_n = 2.22$. We set $a/R_0 = 0.36$, $\rho_* \equiv \rho_{Ti}/a = 1/100$, and $m_i/m_e = 400$. The number of grid points is $512 \times 256 \times 64 \times 16$ for the $(r, \theta, v_\parallel, \mu)$ coordinates, respectively, and the number of toroidal modes is ± 24. Details on the numerical parameters can be found in reference [15].

The equilibrium of the tokamak plasma is axisymmetric, and thus the Fourier decomposition can be applied to fluctuations in the toroidal angle $f = \sum_n f_n \exp(in\zeta)$. The Fourier modes f_n with different n are independent when $|f_n|$ is sufficiently small. When $|f_n|$ becomes large enough, by contrast, the nonlinear term causes coupling between different toroidal modes to exchange the entropy. This nonlinear entropy/free-energy transfer among toroidal modes can be understood by investigating the entropy balance equation for the entropy variable $E_n = \sum_s \int \frac{|\delta f_{s,n}|^2}{2F_{0s}} \mathrm{d}^3v\, \mathrm{d}^3x/(2\pi)$, polarization electrostatic energy $W_{\mathrm{es},n} = \int \frac{1}{2}|\nabla_\perp \phi_n|^2 \mathrm{d}^3x/(2\pi)$ and magnetic energy $W_{\mathrm{em},n} = \int \frac{2}{\beta}|\nabla_\perp A_{\parallel,n}|^2 \mathrm{d}^3x/(2\pi)$ at toroidal wavenumber n

$$\frac{\mathrm{d}}{\mathrm{d}t}\{E_n + W_{\mathrm{es},n} + W_{\mathrm{em},n}\} = T_n + U_n + D_n, \tag{2}$$

where

$$T_n = \sum_{n',n''} T(n; n', n'')\delta_{n,-n'-n''}, \tag{3}$$

U_n is the linear free-energy source originated from L, D_n is the collisional diffusion from C, and $\delta f_s = h_s - \frac{q_s}{T_s}F_{0s}\langle\phi\rangle_s$ is the perturbed distribution function. Details of the definitions of variables are in reference [4]. The nonlinear entropy transfer function is defined by

$$T(n; n', n'') = -\mathrm{Re}\sum_s \int \frac{T_s}{2F_{0s}B}\{S_s(n; n', n'') + S_s(n; n'', n')\}\,\mathrm{d}^3v\,\mathrm{d}^3x, \tag{4}$$

and the nonlinear three-mode-coupling is represented by

$$S_s(n; n', n'') = h_{s,n}[\chi_{s,n'}, h_{s,n''}]. \tag{5}$$

The zonal ($n = 0$) component of equation (2) implies that the nonlinear entropy transfer $T_{n=0}$ is the only free-energy source for zonal-flow excitation, because the $n = 0$ mode is stable against the ITG mode, i.e. $U_{n=0} = 0$.

3. Strong zonal flow excitation at finite β

Figure 1(*a*) shows time history of the electrostatic potential of zonal ($n = 0$) flows and ITG turbulence $\sum_{n\neq 0}\langle|\phi_n|\rangle$ at low-β ($\beta = 0.4\%$) and moderate-β ($\beta = 2.0\%$). It is noted that we use $\beta = 2\beta_i$ instead of β_i used in reference [15]. The ITG turbulence gets saturated by producing zonal flows $\phi_{n=0}$, and then the system reaches a quasi-steady state at $\beta = 2.0\%$ as well as at $\beta = 0.4\%$. This establishment of the steady state of the ITG turbulence at $\beta > 1.2\%$ is in contrast to the non-saturation in the local simulations. The saturation of the ITG turbulence at $\beta = 2.0\%$ is attributed to strong zonal-flow excitation, which is demonstrated by the large amplitude of toroidal mode number spectra of the electrostatic potential at $n = 0$ in figure 1(*b*), and is similar to the electrostatic case [25]. In order to understand the zonal flow excitation, we evaluate the entropy transfer to zonal modes instead of that to zonal flows hereafter, because the ratio of zonal flows to the zonal modes $W_{\mathrm{es},n=0}/(E_{n=0} + W_{\mathrm{es},n=0} + W_{\mathrm{em},n=0}) = 0.013$ at $\beta = 2.0\%$ is similar or even larger than 0.008 at $\beta = 0.4\%$.

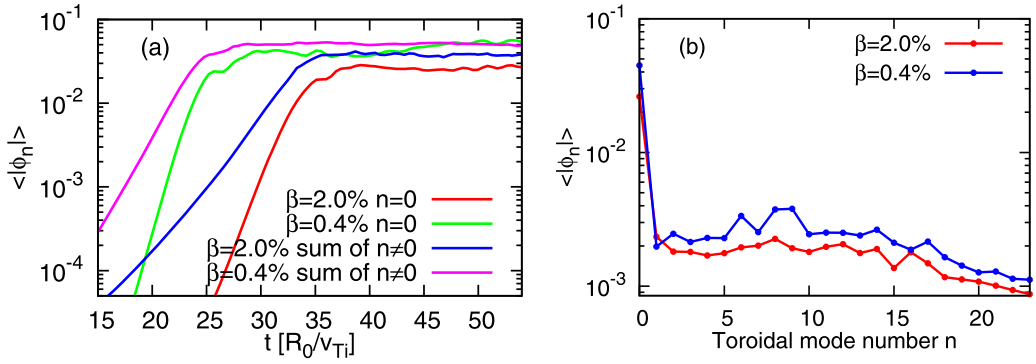

Figure 1. (*a*) Time trace of the electrostatic potential for zonal flows $\langle|\phi_{n=0}|\rangle$ and ITG turbulence $\sum_{n\neq 0}\langle|\phi_n|\rangle$ at $\beta = 2.0\%$ and 0.4%. (*b*) Toroidal mode number spectra of the electrostatic potential averaged over the quasi-steady state at $\beta = 2.0\%$ and 0.4%.

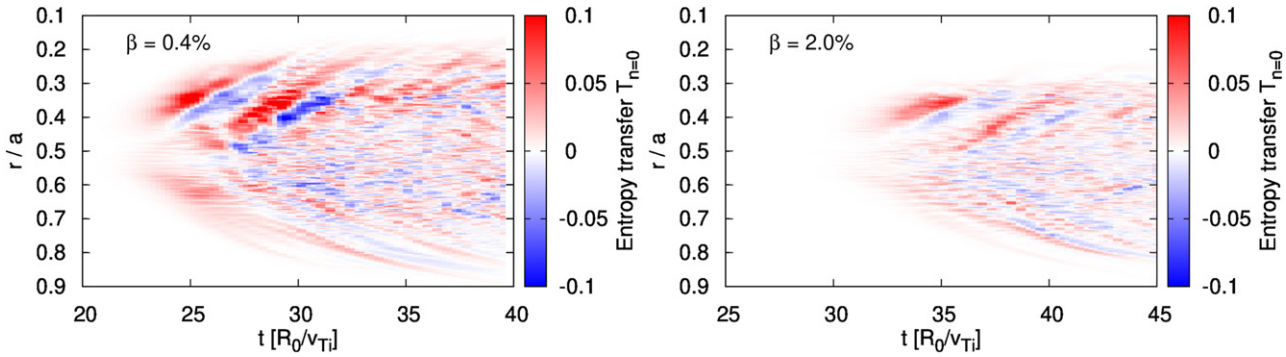

Figure 2. Time trace of the profile of entropy transfer to zonal modes $T_{n=0}(r,t)$ at $\beta = 0.4\%$ and 2.0%.

4. Nonlinear entropy transfer in real space

Here, we investigate the mechanism of the strong zonal-flow excitation that leads to the steady state observed at $\beta = 2.0\%$ by means of the entropy transfer analysis. Figure 2 shows time history of the radial profile of entropy transfer to zonal modes $T_{n=0}(r,t)$, where $T_n = \int T_n(r,t)\mathrm{d}r$. The transfer to $n = 0$ mode is strong at $r \simeq 0.35$ and $r \simeq 0.6$ at both $\beta = 0.4\%$ and 2.0%, while the peak of the amplitude of turbulent fluctuations is located at $r \simeq 0.5$. This implies that the nonlinear excitation of zonal modes $T_{n=0}(r)$ is strong at the both sides of the peak of the ITG turbulence at low-β ($\beta = 0.4\%$) and moderate-β ($\beta = 2.0\%$). In order to elucidate global effects on the zonal-mode excitation, the profile of the entropy transfer and those of electrostatic and magnetic fluctuations averaged over the saturation phase are plotted in figure 3. The entropy transfer to zonal modes is strong at $r \simeq 0.35$ and $r \simeq 0.6$, i.e. at the both sides of the peak of magnetic fluctuations of the turbulence for $\beta = 0.4\%$ and 2.0%, implying that the zonal flow production is not suppressed by the magnetic fluctuations of the turbulence at moderate-β ($\beta = 2.0\%$). As a result, the global zonal flow is strongly excited, leading to the saturation of the ITG turbulence. We also observe the turbulence spreading in the radial direction [26–28] from $t = 24$ to 27 for $\beta = 0.4\%$ and from $t = 33$ to 36 for $\beta = 2.0\%$. During the spreading, the entropy transfer to zonal modes also propagates in the radial direction to keep its location at the front line of the spreading in figure 2, and thus the suppression of the zonal modes due to the magnetic fluctuations is small. Our preliminary analysis on the entropy transfer from zonal flows to the ITG turbulence implies that the turbulence spreading is caused by the entropy transferred from zonal flows, and thus the turbulence spreading is mediated by zonal flows produced by the radial advection of the entropy. In addition, the difference of spreading between density fluctuations δn_n^2 and that of $W_{\mathrm{es},n}$ presented in reference [29] can be investigated by evaluating the Reynolds and Maxwell stresses [30]. We will report them in our next paper.

Here, we discuss the mechanism of the strong entropy transfer at the side of the active region of the turbulence. We can divide the entropy transfer into three parts, because the nonlinear three-mode-coupling in equation (4) can be divided into three terms

$$S_s(n;n',n'') = \nabla\cdot(h_{s,n}h_{s,n''}\langle\tilde{\mathbf{v}}_{E\times B,n'}\rangle_s) + v_{Ts}v_\parallel\langle\tilde{\mathbf{b}}_{n'}\rangle_s\cdot\nabla(h_{s,n}h_{s,n''}) - S_s(n'';n',n) \tag{6}$$

by using $f[g,h] = [g,fh] - h[g,f]$. The first term, which vanishes in local simulations, represents the convected entropy flux by the perturbed $E\times B$ flow $\tilde{\mathbf{v}}_{E\times B} = \frac{-1}{B}\nabla_\perp\phi\times\mathbf{b}$ in real space. The second term, which also vanishes in local simulations, is the entropy flux due to parallel streaming along perturbed field lines $\tilde{\mathbf{b}} = -\mathbf{b}\times\nabla_\perp A_\parallel$, i.e. the magnetic flutter of the entropy. The last term is the transfer to n mode by the loss

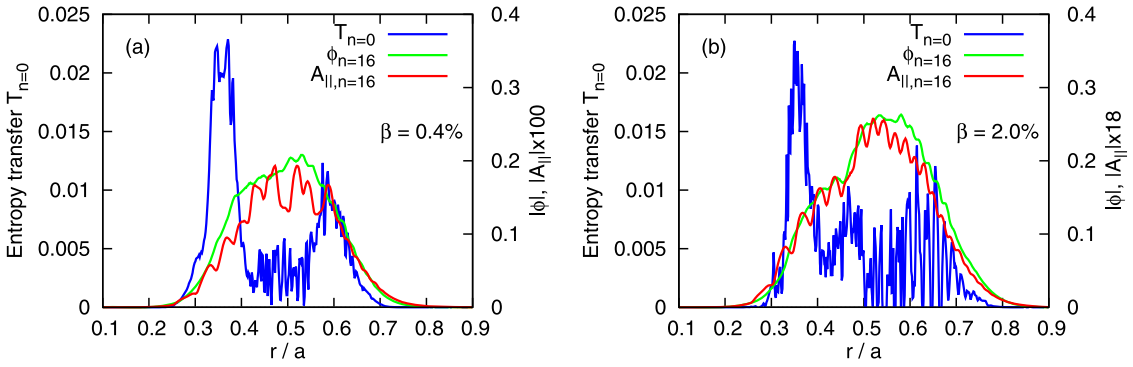

Figure 3. Profile of nonlinear entropy transfer to zonal modes $T_{n=0}(r)$, and the electrostatic and magnetic fluctuations, ϕ and $A_{\parallel}$, of the ITG turbulence for (a) $\beta = 0.4\%$ and (b) $\beta = 2.0\%$.

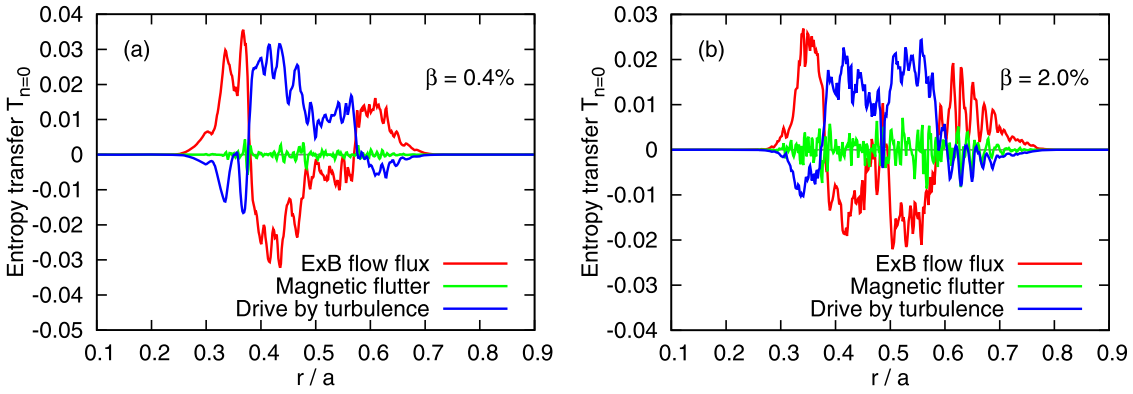

Figure 4. The entropy transfer $T_{n=0}(r,t)$ due to the turbulent $E \times B$ flow convection, due to the magnetic flutter, and the drive from the turbulence for (a) $\beta = 0.4\%$ and (b) $\beta = 2.0\%$.

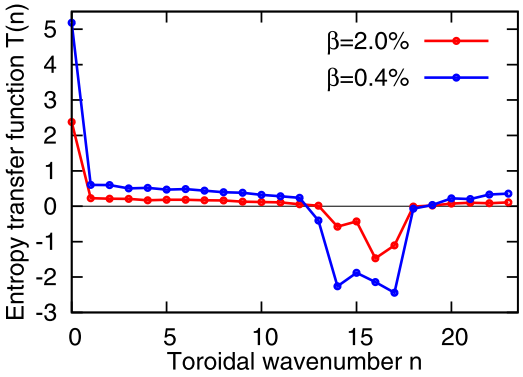

Figure 5. Toroidal mode number spectrum of the nonlinear entropy transfer of ITG turbulence $T_n = \sum_{n',n''} T(n; n', n'')\delta_{n,-n'-n''}$.

of the entropy of n'' mode. For the zonal ($n = 0$) mode production, the first term represents the radial convection of the entropy transferred from the turbulence, the second term is the radial entropy flux by the magnetic flutter, and the last one is the excitation by the lost entropy of the ITG turbulence at $n'' \gg 1$. Figure 4 shows the profile of the entropy transfer to zonal modes $T_{n=0}(r)$ due to these three terms in equation (6) averaged over the saturation phase. The lost entropy of the ITG turbulence (the third term in equation (6)) is positive and peaks at $r \simeq 0.46$ where the peak of the turbulence is located. The radial flux due to the perturbed $E \times B$ flow (the first term in equation (6)) is negative and almost cancels out the drive from the turbulence peaking at $r \simeq 0.46$, while the flux is positive at the both sides of the turbulence $r \simeq 0.36$ and 0.6, and thus the entropy transferred from the ITG turbulence is diffused by the turbulent $E \times B$ flow in the radial direction from the peak of the fluctuations located at $r \simeq 0.5$ to the side of the peak for both $\beta = 0.4\%$ and 2.0%. As a result, the entropy transfer to $n = 0$ mode avoids the influence of the magnetic fluctuations peaking at $r \simeq 0.5$ for $\beta = 2.0\%$ as shown in figure 3. It is noted that the flux by the turbulent $E \times B$ flow is much larger than by the magnetic flutter causing small-scale oscillations in figure 4. Hence, the strong zonal flows are excited at moderate-β ($\beta = 2.0\%$) by the turbulent $E \times B$ flow convection of the entropy in the radial direction. It is noted that the first two terms in equation (6) for $n = 0$ can be combined to the entropy flux due to the generalized potential flow $\mathbf{b} \times \nabla\chi_s$ as

$$\begin{aligned} &\nabla \cdot (h_{s,n=0} h_{s,-n'} \tilde{\mathbf{v}}_{E\times B,n'}) + v_{Ts} v_{\parallel} \tilde{\mathbf{b}}_{n'} \cdot \nabla (h_{s,n=0} h_{s,-n'}) \\ &\quad = \nabla \cdot (h_{s,n=0} h_{s,-n'} \mathbf{b} \times \nabla \chi_{s,n'}) \\ &\quad \approx -\alpha \nabla^2 |h_{s,n'}|^2. \end{aligned} \tag{7}$$

The profile of the entropy transfer by the turbulent $E \times B$ flow convection in figure 4 suggests that the radial flux can be modeled by the diffusion of the entropy of the ITG turbulence $|h_{s,n'}|^2$ that has a similar profile as $|\phi|$ and $|A_{\parallel}|$ in figure 3.

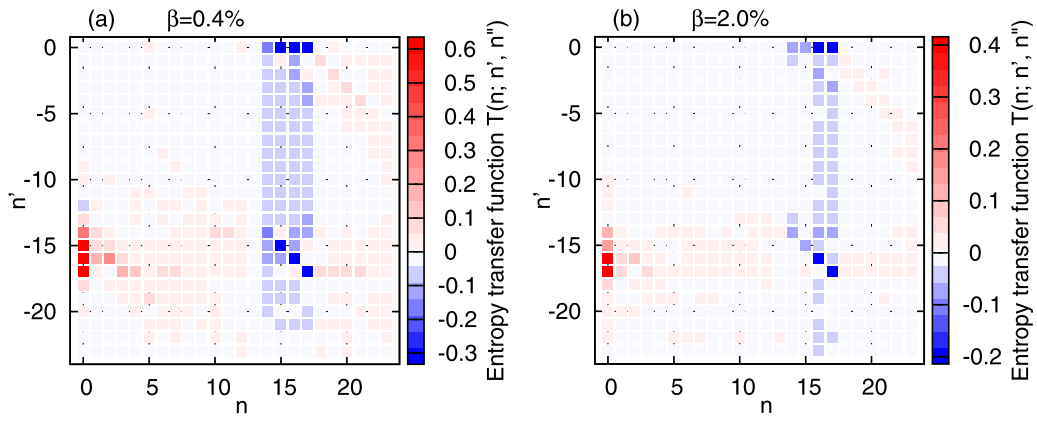

Figure 6. Color map of the entropy transfer function $T(n;\ n', n'')$ of ITG turbulence for (a) $\beta = 0.4\%$ and (b) $\beta = 2.0\%$, where $n + n' + n'' = 0$.

5. Nonlinear entropy transfer in wavenumber space

Finally, we discuss the nonlinear entropy transfer from the unstable ITG mode to stable modes other than the zonal modes, which can be another player causing the saturation of the ITG turbulence, by utilizing the detailed balance relation of the nonlinear entropy transfer function

$$T(n; n', n'') + T(n'; n'', n) + T(n''; n, n') = 0, \qquad (8)$$

where $n + n' + n'' = 0$. Figure 5 shows toroidal mode number spectrum of the entropy transfer $T_n = \sum_{n',n''} T(n;\ n', n'')\delta_{n,-n'-n''}$ averaged over the saturation phase as well as over the radial direction. The importance of the radial advection in the entropy transfer from the turbulence to zonal flow is presented above. Furthermore, the radial dependence of the entropy transfer to the turbulence suggests that the turbulence spreading is mediated by zonal flows excited by the radial convection of the entropy, which is shown our preliminary analysis and will be reported in our next paper. The turbulence loses the entropy around $n = 16$, and the zonal $(n = 0)$ modes obtain most of the entropy, and thus most of the entropy/free-energy of strongly unstable ITG modes at $14 \leqslant n \leqslant 17$ is transferred to zonal modes. In addition, low n modes obtain the entropy, indicating the entropy transfer to stable modes other than the zonal modes. The details of the transfer are shown by the color map of the nonlinear entropy transfer function on the toroidal mode number plane (n, n') in figure 6. The large loss of the entropy at $(n, n') = (15, 0)$, $(16,\ 0)$ and $(17,\ 0)$ indicates that the dominant ITG modes mainly lose the entropy by the interaction with the zonal $(n = 0)$ modes, and correspondingly the zonal modes obtain large amount of entropy at $(n, n') = (0, -15)$, $(0,\ -16)$ and $(0,\ -17)$ as equation (8) is reduced to, for instance, $T(0; -16, 16) = -2T(16;\ 0, -16)$ by using $T(-n; -n', -n'') = T(n; n', n'')$ and $T(n; n'', n') = T(n; n', n'')$. Thus, the most of the entropy of the ITG mode at $n = 15$, 16 and 17 is transferred to the zonal $(n = 0)$ modes, implying that the saturation of the ITG turbulence is mainly caused by the nonlinear interactions with the zonal flows. There is another loss of the entropy at $(n, n') = (16, -2)$, and correspondingly the $n = 2$ mode obtains the entropy at $(n, n') = (2, -16)$. This implies that the entropy transfer to low-n stable modes also plays a role in the saturation of the ITG turbulence. This entropy transfer to low-n stable modes is also the missing mechanism of the saturation in the local simulations that assume the high-n ballooning representation.

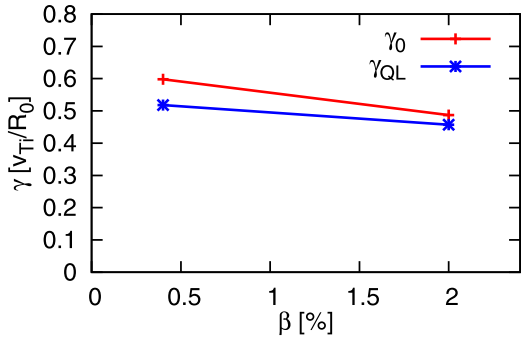

Figure 7. Linear growth rate of the ITG mode $(n = 16)$ for the initial profile γ_0 and for the relaxed profile γ_{QL}.

Lastly, we show that the influence of the profile relaxation on the saturation of the ITG turbulence is small. Figure 7 shows the linear growth rate of the ITG mode $(n = 16)$ for the initial profile γ_0 and that for the relaxed profile γ_{QL}. The relaxed profile is evaluated by averaging from $t = t_1$ to $t = t_2$, where $\frac{1}{|\phi(\mathbf{x},t)|}\frac{\mathrm{d}|\phi(\mathbf{x},t)|}{\mathrm{d}t} = \gamma_0/2$ at $t = t_1$ and $\frac{\mathrm{d}|\phi(\mathbf{x},t)|}{\mathrm{d}t} = 0$ at $t = t_2$. The difference between γ_0 and γ_{QL} is small for $\beta = 0.4\%$ and 2.0%, and thus the nonlinear entropy transfer from ITG turbulence to zonal flow is the dominant saturation mechanism of the ITG turbulence.

6. Summary

Turbulence in finite normalized pressure (β) is electromagnetic and often exhibits non-saturation due to a lack of zonal flows in gyrokinetic simulations using radially localized flux tube geometry. The non-saturation is due to the suppression effect of magnetic fluctuations on zonal flows and is known as the run-away/non-zonal-transition. It is found that ITG turbulence gets saturated at moderate-β in global gyrokinetic

simulations, and the saturation mechanism is revealed by analysis of the nonlinear entropy/free-energy transfer. The entropy transfer analysis in the toroidal mode number space demonstrates that the ITG turbulence gets saturated by the interplay with global zonal ($n = 0$) flows. The zonal flow excitation is not suppressed by the magnetic fluctuations, because the radial location of the entropy transfer to zonal flows avoids the peak of the magnetic fluctuations. The radial shift of the entropy transfer is caused by the turbulent $E \times B$ flow convection of the entropy in real space. The turbulent $E \times B$ flow spreads the entropy of the ITG turbulence away from the peak of the magnetic fluctuations to the side of the peak in the radial direction. Thus, the radial turbulent $E \times B$ flow convection of the entropy is the mechanism of the strong zonal-flow excitation in the global simulations. In addition, analysis of the entropy transfer in the wavenumber space shows that the ITG turbulence gets saturated by the interplay not only with the zonal ($n = 0$) flows but also with stable modes at low toroidal mode number. Hence, these two global saturation mechanisms: the strong zonal-flow excitation by the turbulent $E \times B$ convection of the entropy in the radial direction and the entropy transfer to low-n stable modes, are the saturation physics of the ITG turbulence at moderate-β.

Here, we discuss the ρ^* dependence of ITG turbulence in global simulations. In addition to the zonal flow excitation due to the radial advection of the entropy presented in this letter, there is another suppression mechanism leading the reduction of turbulent transport in small $1/\rho^*$ regime. As $1/\rho^*$ increases, the heat diffusion calculated by global simulations tends to the value evaluated by local simulations from lower values [31], and this suppression effect on the turbulence at smaller $1/\rho^*$ is mainly due to the reduction of the linear growth rate of the ITG mode [32]. This suppression effect at smaller $1/\rho^*$ regime can move up the critical β for the non-zonal-transition/run-away to the MHD instability limit, because the increase of $1/\rho^*$ makes ITG modes unstable at high n, and high wavenumber modes can cause the non-zonal-transition/run-away as suggested in reference [9]. We expect that the radial convection of the entropy does not depend on ρ^*, and will carry out simulations with larger $1/\rho^*$ to clarify the dominant mechanism of the saturation of the ITG turbulence at finite β in larger $1/\rho^*$ regime in our future work.

It is also found that the KBM turbulence at high-β ($\beta > 3\%$) exhibits a similar saturation due to the global production of zonal modes through the turbulent $E \times B$ flow convection of the entropy in the radial direction, while the zonal pressure plays more important role. We will report details of these results on the KBM turbulence in a separate paper.

Acknowledgments

This work was supported by the Japanese Ministry of Education, Culture, Sports, Science and Technology, Grant No. 17K06991. Simulations are performed on Plasma Simulator supercomputer at NIFS and JFRS-1 supercomputer at QST.

ORCID iDs

H. Masui https://orcid.org/0000-0002-7911-2974
A. Ishizawa https://orcid.org/0000-0002-5323-8448

References

[1] Candy J. 2005 *Phys. Plasmas* **12** 072307
[2] Pueschel M.J., Kammerer M. and Jenko F. 2008 *Phys. Plasmas* **15** 102310
[3] Pueschel M.J. and Jenko F. 2010 *Phys. Plasmas* **17** 062307
[4] Ishizawa A., Maeyama S., Watanabe T.-H., Sugama H. and Nakajima N. 2015 *J. Plasma Phys.* **81** 435810203
[5] Staebler G.M. 2018 *Nucl. Fusion* **58** 115001
[6] Whelan G.G., Pueschel M.J. and Terry P.W. 2018 *Phys. Rev. Lett.* **120** 175002
[7] Howes G.G., TenBarge J.M., Dorland W., Quataert E., Schekochihin A.A., Numata R. and Tatsuno T. 2011 *Phys. Rev. Lett.* **107** 035004
[8] Pueschel M.J., Jenko F., Told D. and Buchner J. 2011 *Phys. Plasmas* **18** 112102
[9] Waltz R.E. 2010 *Phys. Plasmas* **17** 072501
[10] Pueschel M.J., Terry P.W., Jenko F., Hatch D.R., Nevins W.M., Gorler T. and Told D. 2013 *Phys. Rev. Lett.* **110** 155005
[11] Pueschel M.J., Terry P.W. and Hatch D.R. 2014 *Phys. Plasmas* **21** 055901
[12] Terry P.W., Pueschel M.J., Carmody D. and Nevins W.M. 2013 *Phys. Plasmas* **20** 112502
[13] Hatch D.R., Pueschel M.J., Jenko F., Nevins W.M., Terry P.W. and Doerk H. 2012 *Phys. Rev. Lett.* **108** 235002
[14] Dong G., Bao J., Bhattacharjee A. and Lin Z. 2019 *Phys. Plasmas* **26** 010701
[15] Ishizawa A., Imadera K., Nakamura Y. and Kishimoto Y. 2019 *Phys. Plasmas* **26** 082301
[16] Urano H., Takizuka T., Takenaga H., Oyama N., Miura Y. and Kamada Y. 2006 *Nucl. Fusion* **46** 781
[17] Vermare L. *et al* (The ASDEX Upgrade Team) 2007 *Nucl. Fusion* **47** 490
[18] Petty C.C. 2008 *Phys. Plasmas* **15** 080501
[19] McDonald D.C. *et al* (JET EFDA Contributors) 2008 *Plasma Phys. Control. Fusion* **50** 124013
[20] Challis C.D. *et al* 2015 *Nucl. Fusion* **55** 053031
[21] Imadera K., Kishimoto Y., Obrejan K., Kobiki T. and Li J.Q. 2014 Global profile relaxation coupled with $E \times B$ staircase in toroidal flux-driven ITG turbulence *25th IAEA Int. Conf. on Fusion Energy* (St Petersburg) [TH/P5-8]
[22] Obrejan K., Imadera K., Li J.Q. and Kishimoto Y. 2017 *Comput. Phys. Commun.* **216** 8
[23] Hahm T.S., Lee W.W. and Brizard A. 1988 *Phys. Fluids* **31** 1940
[24] Dimits A.M. *et al* 2000 *Phys. Plasmas* **7** 969
[25] Wang W., Kishimoto Y., Imadera K., Li J.Q. and Wang Z.X. 2018 *Nucl. Fusion* **58** 056005
[26] Kishimoto Y., Tajima T., Horton W., LeBrun M.J. and Kim J.Y. 1996 *Phys. Plasmas* **3** 1289
[27] Miki K., Kishimoto Y., Miyato N. and Li J.Q. 2007 *Phys. Rev. Lett.* **99** 145003
[28] Hahm T.S. and Diamond P.H. 2018 *J. Korean Phys. Soc.* **73** 747
[29] Gurcan O.D., Diamond P.H. and Hahm T.S. 2006 *Phys. Rev. Lett.* **97** 024502
[30] Ishizawa A., Urano D., Nakamura Y., Maeyama S. and Watanabe T.-H. 2019 *Phys. Rev. Lett.* **123** 025003
[31] McMillan B.F., Lapillonne X., Brunner S., Villard L., Jolliet S., Bottino A., Gorler T. and Jenko F. 2010 *Phys. Rev. Lett.* **105** 155001
[32] Gorler T., Lapillonne X., Brunner S., Dannert T., Jenko F., Merz F. and Told D. 2011 *J. Comput. Phys.* **230** 7053